may result from elastic momentum transfer or charge exchange collisions. This second distribution is obscured in the LIF spectra by broadening and hyperfine structure. For this analysis, only the characteristics of the larger peak in the MBMS energy distribution were considered.

The MBMS velocity distribution peaked at 18.9 ± 0.4 km/s, and the energy distribution peaked at 230 ± 10 eV corrected for plasma potential with a FWHM of 20 eV. The bulk axial velocity given by LIF is 7.4% less than the MBMS peak velocity. This difference is too great for the uncertainty in angle α. The difference may result from noise-related fitting errors of the LIF data (potentially as large as 10% uncertainty, or 1500 m/s), incorrect estimation of the plasma potential in the MBMS data reduction, chamber effects in the MBMS data, or a combination of these. Applying Eq. (6) to the MBMS energy distribution yields a temperature of 2500 K.

Neither axial temperature measurement shows the drastic cooling predicted by collisionless acceleration theory. From Eq. (11), a divergence of 35 ± 6 deg, which is consistent with LIF velocity mapping off the centerline of the discharge annulus,[5] yields the temperature measured by LIF. Beam divergence, plasma oscillations, and electron-neutral collisions may also offset any acceleration cooling, and the measured temperature probably results from a complex combination of effects.

The MBMS temperature is roughly 41% of the LIF axial temperature. This difference may result from the non-Maxwellian nature of the data and/or saturation broadening of the LIF data. Whereas the scarcity of data in the MBMS peak introduces uncertainty in the evaluation of Eq. (5), a distribution with a temperature of 6500 K is a poor fit of the data. An improved deconvolution model is needed to increase the accuracy of velocity and energy distributions measured with LIF.

Conclusions

The spread in the ion energy distribution obtained from LIF data is comparable to that obtained from MBMS data given the uncertainties in both techniques involved. The ion temperatures calculated from the two techniques were of the same order of magnitude and indicate significant beam divergence. The primary differences associated with these techniques that are stated in the literature are not actually present. The MBMS is not artificially broadening the signal due to the collection of crossflowing ions, and the LIF signal is neither from a sparsely populated electronic state nor from an interrogation spot too small to capture the velocity profile.

References

[1]King, L. B., and Gallimore, A. D., "Transport-Property Measurements in the Plume of an SPT-100 Hall Thruster," *Journal of Propulsion and Power*, Vol. 14, No. 3, 1998, pp. 327–335.

[2]Manzella, D. H., "Stationary Plasma Thruster Ion Velocity Distribution," AIAA Paper 94-3141, June 1994.

[3]Gulczinski, F. S., and Gallimore, A. D., "Near-Field Ion Energy and Species Measurements of a 5-kW Laboratory Hall Thruster," AIAA Paper 99-2430, June 1999.

[4]Domonkos, M. T., Marrese, C. M., Haas, J. M., and Gallimore, A. D., "Very Near-Field Plume Investigation of the D-55," AIAA Paper 97-3062, July 1997.

[5]Williams, G. J., Smith, T. B., Gulczinski, F. S., Beal, B. E., Gallimore, A. D., and Drake, R. P., "Laser-Induced Fluorescence Measurement of Ion Velocities in the Plume of a Hall Effect Thruster," AIAA Paper 99-2424, June 1999.

[6]Williams, G. J., Smith, T. B., Gulczinski, F. S., Beal, B. E., Gallimore, A. D., and Drake, R. P., "Laser-Induced Fluorescence Characterization of Ions Emitted from Hollow Cathodes," AIAA Paper 99-2862, June 1999.

[7]Kameyama, I., and Wilbur, J. P., "Characteristics of Ions Emitted from High-Current Hollow Cathodes," *Proceedings of the International Electric Propulsion Conference*, IEPC Paper 93-023, Aug. 1993.

[8]Hargus, W. A., and Cappelli, M. A., "Interior and Exterior Laser-Induced Fluorescence and Plasma Potential Measurements on a Laboratory Hall Thruster," AIAA Paper 99-2721, June 1999.

[9]Keefer, D., Wright, N., Hornkohl, J., and Bangasser, J., "Multiplexed LIF and Langmuir Probe Diagnostic Measurements in the TAL D-55 Thruster," AIAA Paper 99-2425, June 1999.

[10]Gombosi, T. I., *Gaskinetic Theory*, Cambridge Univ. Press, New York, 1994, pp. 39, 40.

[11]Dressler, R. A., Beijers, J. P. M., Meyer, H., Penn, S. M., Bierbaum, V. M., and Leone, S. R., "Laser Probing of Ion Velocity Distributions in Drift Fields: Parallel and Perpendicular Temperatures and Mobility for Ba^+ in He," *Journal of Chemical Physics*, Vol. 89, No. 8, 1988, p. 4707.

[12]Kaufman, S. L., "High-Resolution Laser Spectroscopy in Fast Beams," *Optics Communications*, Vol. 17, No. 3, 1976, pp. 309–312.

[13]Meehan, N. B., Schmidt, D. P., Hargus, W. A., and Cappelli, M. A., "Optical Study of Anomalous Electron Transport in a Laboratory Hall Thruster," AIAA Paper 99-2284, June 1999.

[14]Haas, J. M., and Gallimore, A. D., "An Investigation of Internal Ion Number Density and Electron Temperature Profiles in a Laboratory-Model Hall Thruster," AIAA Paper 2000-3422, July 2000.

Transonic Rotor Blade Pressure Measurement Using Fluorescent Paints

T. Liu*
NASA Langley Research Center, Hampton, Virginia 23681
S. Torgerson†
LM Aero, Palmdale, California 93550
J. Sullivan‡
Purdue University, West Lafayette, Indiana 47907
R. Johnston§
Pratt & Whitney, Middletown, Connecticut 06457
and
S. Fleeter¶
Purdue University, West Lafayette, Indiana 47907

Nomenclature

A	=	constant in Stern–Volmer relation
B	=	constant in Stern–Volmer relation
C	=	rotor chord
E	=	Arrhenius activation energy
I	=	measured luminescent intensity
p	=	pressure
R	=	radial location
Rg	=	universal gas constant
T	=	temperature, K
X	=	chordwise distance

Subscripts

hub	=	value at hub location
ref	=	reference value
0	=	stagnation value

Introduction

PRESSURE and temperature-sensitive paints have been utilized for the measurement of blade surface pressure and temperature in a high-speed axial compressor environment. Four blades were painted: two with temperature sensitive paints and two with pressure sensitive paints allowing pressure distributions to be corrected for paint sensitivity to temperature variations. Pressure maps on the

Received 16 September 2000; revision received 5 July 2001; accepted for publication 20 October 2001.

*Research Scientist, Model Systems. Member AIAA.
†Engineer, Test. Member AIAA.
‡Professor, School of Aeronautics and Astronautics. Senior Member AIAA.
§Instrumentation Technology Manager. Senior Member AIAA.
¶McAllister Distinguished Professor, School of Mechanical Engineering. Fellow AIAA.

suction surface of a blade were obtained over a range of rotational speeds. The formation of a suction surface shock was detected at the higher speeds.

Experimental Facility

The Purdue Research Axial Fan Facility features a 30.48-cm (12-in.)-diam, 2/3 hub-tip ratio compressor rotor, which is integral with the shaft. This facility is representative of modern gas turbine engines in that it has low-aspect-ratio blades and can operate at transonic flow conditions. This makes it a good test bed for the evaluation of PSP and TSP for use in gas turbine engines. For more details on this facility, see Ref. 1.

PSP and TSP Theory and Measurement Techniques

The physical processes involved in behavior of PSP and TSP have been thoroughly presented in literature.[2–4] A probe molecule embedded in a polymer binder is elevated to an excited state by absorbing light of a particular wavelength. The molecule will return to the ground state by releasing the energy via emission of light (fluorescence and phosphorescence) or through radiationless deactivation processes such as oxygen quenching and thermal quenching. Oxygen quenching depends upon the concentration of oxygen molecules, which is proportional to the partial pressure of oxygen. Hence, for pressure sensitive paint luminescence is sensitive to pressure and can be modeled with the Stern–Volmer relation:

$$I_{\text{ref}}/I = A(T) + B(T)(p/p_{\text{ref}}) \tag{1}$$

where A and B are the coefficients to be determined experimentally.

Temperature-sensitive paints (TSPs) reduce energy levels through radiationless transitions (that is, vibrational and rotational motions of the molecule). The temperature dependence of luminescent intensity can be described by the simple Arrhenius relation over a certain temperature range:

$$\ell n\left[\frac{I(T)}{I_{\text{ref}}(T_{\text{ref}})}\right] = \frac{E}{R_g}\left(\frac{1}{T} - \frac{1}{T_{\text{ref}}}\right) \tag{2}$$

In intensity-based PSP and TSP measurements a reference signal [image for a charge-coupled device (CCD) camera system] is taken prior to the experiment starting. This "wind off" or reference signal is ratioed with the signal taken under test conditions. Ratioing the signals removes nonuniformities in luminescence caused by illumination and uneven paint thickness.

The PSP used in this study is Ru(ph2-phen) + silica gel particles in GE RTV 118. It was calibrated over a range of temperatures useful in rotating machinery.[2] The temperature-dependent Stern–Volmer coefficients are $A(T) = a_0 + a_1 T$ and $B(T) = b_0 + b_1 T$, where $a_0 = 0.099937, a_1 = 1.2333 \times 10^{-3}, b_0 = 0.5581, b_1 = 0.01262$, and T is in Celsius. The TSP used is Ru(bpy) in Shellac. The constant E/Rg is 1,070 for Ru(bpy)-Shellac paint. The PSP and TSP were coated on alternating blades by dipping the blades in the paint, resulting in a thickness of approximately 20 μ.

Instead of a CCD camera system commonly used for TSP and PSP measurements in wind tunnels, a laser scanning system was adopted for measurements in the compressor where optical access is very limited.[3] The laser scanning system used is shown in Fig. 1. An air-cooled Argon laser with filtered output of 488 nm was used as an illumination source for both the PSP and TSP. It was mounted upstream of the inlet contraction in order to illuminate the moving rotor blades. Using a computer-controlled scanning mirror, the 1-mm-diam laser spot was scanned to 21 spanwise locations over each blade. Luminescence was detected with a Hamamatsu photomultiplier tube after the excitation light was filtered from the signal with a long-pass optical filter. Data were collected using a PC with a 12-bit analog-to-digital converter operating at a maximum of 500 KSamples/s. There was a minimum of 100 data points in the chordwise direction and 50 rotor revolutions were ensemble averaged to remove unsteady effects.

Results

To calculate temperature and pressure, the signal at the lowest speed of 1,000 rpm was used as the wind-off intensity. As the pressure and temperature on the surface varies as rotational speed squared, the error in using this is less than 1% for the speeds utilized in this sturdy. Figure 1 shows spanwise surface temperature distributions at midchord at different rotational speeds. Surface temperatures are higher at larger radial distances because the relative velocity is greater there. This is consistent with the distributions of the relative Mach numbers.[2]

Figure 2 shows the normalized chordwise pressure distributions (p/p_0) at 75% span for different rotational speeds, where p_0 is the upstream stagnation pressure (1 atm in this case). Again, the formation of a shock is evidenced by the abrupt increase in the pressure distribution. As the rotational speed increases, the strength of the shock becomes larger, and its location moves downstream.

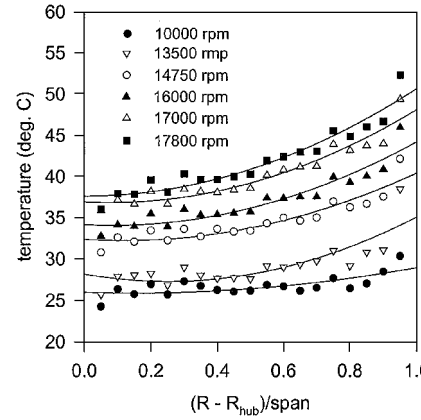

Fig. 2 Spanwise surface temperature distribution at 10,000; 13,500; 14,750; 16,000; 17,000; and 17,800 rpm.

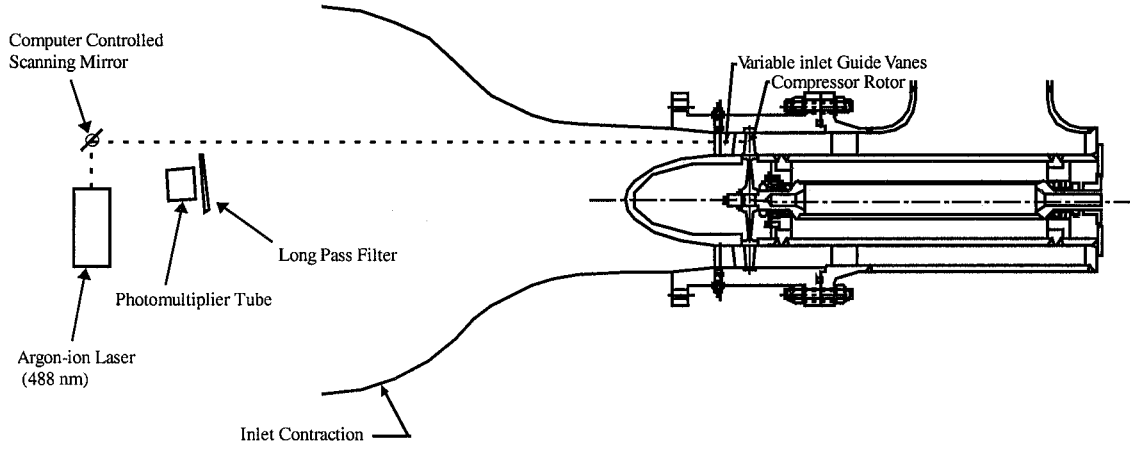

Fig. 1 Compressor facility showing optical access for pressure and temperature paint measurement.

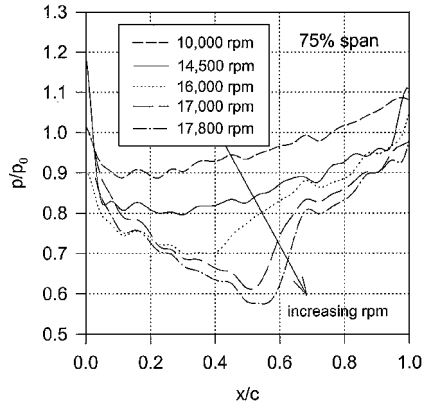

Fig. 3 PSP pressure distributions at 75% span.

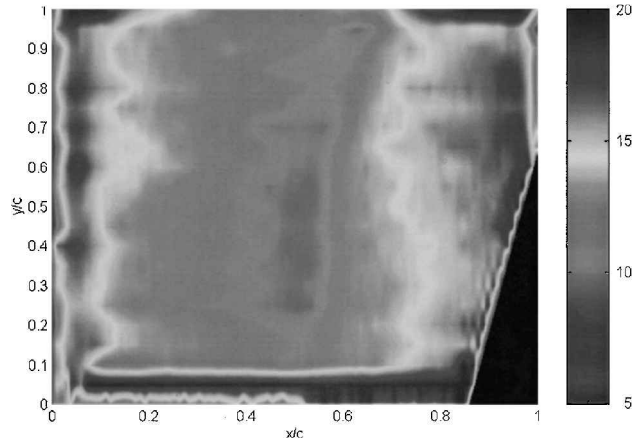

Fig. 4 Suction surface-pressure map at 17,500 rpm.

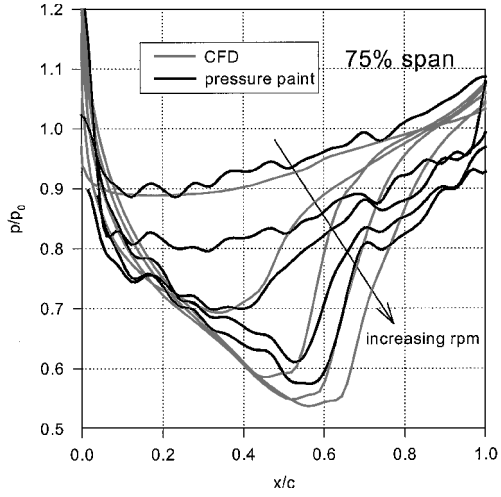

Fig. 5 Comparison between CFD results and PSP data at 75% span 10,000; 14,750; 16,000; 17,000; and 17,800 rpm.

Figure 3 shows a surface-pressure map at 17,800 rpm. This two-dimensional maps clearly indicate the formation of a shock that produces a rapid pressure rise across it Fig. 4. The black patch at the right edge results from blade overlap near the root.

A cascade analysis was performed at the 0.75 span of the rotor blade using Rotor Viscous Code Quasi-3D from R. Chima at NASA Lewis Research Center.[5] This Navier–Stokes code incorporates a Baldwin–Lomax turbulence model. Figure 5 shows comparison between computational fluid dynamics (CFD) results and PSP data at 75% span for different rotational speeds. The PSP-derived pressure distributions exhibit the same trend as those given by the CFD code. Quantitatively, the measured pressure data are lower than the CFD results.

Conclusions

Pressure- and temperature-sensitive paints have been used for the measurement of blade surface-pressure and temperature distributions in a high-speed axial compressor environment. Measurements of the suction surface pressure were made from the hub to tip in several rotational speeds. The two-dimensional surface pressure maps clearly indicate the presence of a shock wave at higher rotational speeds, which is not evident in the corresponding temperature maps.

References

[1]Johnston, R. T., and Fleeter, S., "Time Resolved Variations of an IGV Flow Field in the Presence of a Rotor Potential Field," AIAA Paper 96-2670, July 1996.

[2]Lui, T., Torgerson, S., Johnston, R., Fleeter, S., and Sullivan, J., "Rotor Blade Pressure Measurement in a High Speed Axial Compressor Using Pressure and Temperature Sensitive Paints," AIAA Paper 97-0162, Jan. 1997.

[3]Torgerson, S. D., "A Laser Scanning System for Use with Pressure and Temperature Sensitive Paints," Master's Thesis, School of Aeronautics and Astronautics, Purdue Univ., West Lafayette, IN, Aug. 1997.

[4]McLachlan, B. G., Kavandi, J. L., Callis, J. B., Gouterman, M., Green, E., and Khalil, G., "Surface Pressure Field Mapping Using Luminescent Coatings," *Experiments in Fluids*, Vol. 14, 1993, pp. 33–41.

[5]Chima, R. V., "Explicit Multigrid Algorithm for Quasi-Three-Dimensional Viscous Flows in Turbomachinery," *Journal of Propulsion and Power*, Vol. 3, No. 5, 1987, pp. 397–405.

Unsteady Flow in a Supersonic Turbine with Variable Specific Heats

Daniel J. Dorney* and Lisa W. Griffin†
NASA Marshall Space Flight Center,
Marshall Space Flight Center, Alabama 35812
Frank Huber‡
Riverbend Design Services, Palm Beach Gardens, Florida 33418
and
Douglas L. Sondak§
Boston University, Boston, Massachusetts 02215

Introduction

MODERN high-work turbines can be compact, transonic, supersonic, counter-rotating, or use a dense drive gas. The vast majority of modern rocket turbine designs fall into these categories. These turbines usually have large temperature variations across a given stage and are characterized by large amounts of flow unsteadiness. The flow unsteadiness can have a major impact on the turbine performance and durability. For example, the space transportation main engine fuel turbine, a high-work, transonic design, was found to have an unsteady interrow shock that reduced efficiency by two

Received 15 June 2001; revision received 16 September 2001; accepted for publication 2 October 2001.

*Aerospace Engineer, Applied Fluids Dynamic Analysis Branch. Senior Member AIAA.

†Team Leader, Applied Fluids Dynamic Analysis Branch. Senior Member AIAA.

‡President. Senior Member AIAA.

§Senior Scientific Programmer, Office of Information Technology. Senior Member AIAA.